NACA

RESEARCH MEMORANDUM

AN INVESTIGATION AT MACH NUMBERS OF 1.40 AND 1.59 OF THE EFFECTS OF AILERON PROFILE ON THE AERODYNAMIC CHARACTERISTICS OF A COMPLETE MODEL OF A SUPERSONIC AIRCRAFT CONFIGURATION

By M. Leroy Spearman and Robert A. Webster

Langley Aeronautical Laboratory
Langley Field, Va.

NATIONAL ADVISORY COMMITTEE
FOR AERONAUTICS

WASHINGTON
January 15, 1951

Classification cancelled (or changed to UNCLASSIFIED)

By Authority of NASA Tech Pub Announcement #128
(OFFICER AUTHORIZED TO CHANGE)

By 28 Jul 65
NAME AND

GRADE OF OFFICER MAKING CHANGE)

27 Mar 64
DATE

NATIONAL ADVISORY COMMITTEE FOR AERONAUTICS

RESEARCH MEMORANDUM

AN INVESTIGATION AT MACH NUMBERS OF 1.40 AND 1.59 OF THE EFFECTS OF AILERON PROFILE ON THE AERODYNAMIC CHARACTERISTICS OF A COMPLETE MODEL OF A SUPERSONIC AIRCRAFT CONFIGURATION

By M. Leroy Spearman and Robert A. Webster

SUMMARY

An investigation has been conducted in the Langley 4- by 4-foot supersonic tunnel at Mach numbers of 1.40 and 1.59 to determine the effect of aileron profile on the aerodynamic characteristics of a complete model of a supersonic aircraft configuration. The model had a 40° swept-back tapered wing with 10-percent-thick circular-arc sections normal to the quarter-chord line. The ailerons were 20-percent chord and were located on the outboard 50 percent of the wing semispans. The various ailerons investigated included the basic circular-arc profile and three flat-sided ailerons having ratios of trailing-edge thickness to hinge-line thickness t of 0, 0.5, and 1.0.

Low aileron effectiveness was obtained with the circular-arc and $t = 0$ profiles. Increasing the trailing-edge thickness ($t = 0.5$ and 1.0) resulted in increased effectiveness as well as increased hinge moments with only a slight increase in drag.

The aileron lift effectiveness C_{L_δ} was in reasonably good agreement with theory although the variations of rolling- and hinge-moment coefficient with aileron deflection, C_{l_δ} and C_{h_δ}, were, in general, somewhat less than that predicted by theory. The variation of C_{l_δ}, C_{h_δ}, and C_{L_δ} with trailing-edge angle for the various aileron profiles agreed well with the theoretical results.

INTRODUCTION

An extensive investigation has been conducted by the National Advisory Committee for Aeronautics to determine the characteristics of various lateral-control devices on a wing having 40° of sweepback at the quarter-chord line, aspect ratio 4, taper ratio 0.5, and symmetrical 10-percent-thick circular-arc sections in a plane normal to the quarter-chord line.

Rocket model tests of such a wing equipped with 20-percent-chord, 50-percent-span outboard, true-contour (circular-arc) ailerons indicated roll reversal for small aileron deflections in the transonic-speed range (reference 1). In an effort to develop a suitable control for the transonic-speed range, several lateral-control devices and various aileron modifications were investigated by the transonic-bump method (references 2 and 3), and in flight using the rocket-model technique (reference 4). Modifications made to the aileron included flattening the sides of the circular-arc profile and increasing the trailing-edge thickness of the aileron. The flat-sided ailerons with thickened trailing edges eliminated the roll reversal in the transonic range.

Some of the controls developed were also investigated at a Mach number of 1.9 in the Langley 9- by 12-inch supersonic blowdown tunnel (references 5, 6, and 7). The results at this Mach number indicated positive rolling effectiveness for all ailerons tested with the thickened trailing-edge profiles showing some increase in effectiveness over that of the circular-arc profile.

The damping-in-roll characteristics of the wing in the transonic range and at a Mach number of 1.9 were reported in reference 8. In addition, some subsonic characteristics of the circular-arc profile aileron have been obtained from tests of a complete model in the Langley 300 MPH 7- by 10-foot tunnel and are reported in reference 9.

The present paper contains the results of an investigation conducted at Mach numbers of 1.40 and 1.59 in the Langley 4- by 4-foot supersonic tunnel to determine the characteristics of a complete model equipped with various ailerons, the circular-arc profile and three flat-sided ailerons having ratios of trailing-edge thickness to hinge-line thickness of 0, 0.5, and 1.0. These results include six-component measurements for the complete model as well as aileron hinge-moment measurements. For comparison, theoretical estimates of some of the aileron characteristics are included.

SYMBOLS

The results of the tests are presented as standard NACA coefficients of forces and moments. The data are referred to the stability axes system (fig. 1) with the reference center of gravity at 25 percent of the mean aerodynamic chord (see fig. 2).

The coefficients and symbols are defined as follows:

C_L	lift coefficient (Lift/qS where Lift = -Z)
C_D	drag coefficient (Drag/qS where Drag = -X)
C_Y	lateral-force coefficient (Y/qS)
C_l	rolling-moment coefficient (L/qSb)
C_m	pitching-moment coefficient ($M'/qS\bar{c}$)
C_n	yawing-moment coefficient (N/qSb)
C_h	hinge-moment coefficient ($H/2qM_a$)
Z	force along Z-axis, pounds
X	force along X-axis, pounds
Y	force along Y-axis, pounds
L	moment about X-axis, pound-feet
M'	moment about Y-axis, pound-feet
N	moment about Z-axis, pound-feet
H	aileron hinge moment about hinge line, pound-feet
q	free-stream dynamic pressure, pounds per square foot $\left(\frac{1}{2}\rho V^2\right)$
S	total wing area, square feet
b	wing span, feet
$\bar{c}$	wing mean aerodynamic chord, feet $\left(\frac{2}{S}\int_0^{b/2} c^2 dy\right)$

M_a	moment area of the aileron about hinge line
$pb/2V$	wing-tip helix angle generated by wing tip in roll, radians
p	rolling angular velocity, radians per second
V	free-stream airspeed, feet per second
ρ	mass density of air, slugs per cubic feet
c	airfoil-section chord, feet
y	distance along wing span, feet
α	angle of attack of fuselage center line, degrees
ψ	angle of yaw, degrees
ϕ	trailing-edge angle of aileron in free-stream direction, degrees
i_t	stabilizer incidence angle with respect to fuselage center line, degrees
δ_a	aileron deflection in free-stream direction, degrees
t	ratio of aileron trailing-edge thickness to hinge-line thickness
C_{l_δ}	rate of change of rolling-moment coefficient with aileron deflection $(\partial C_l/\partial \delta_a)$
C_{h_δ}	rate of change of hinge-moment coefficient with aileron deflection $(\partial C_h/\partial \delta_a)$
C_{h_α}	rate of change of hinge-moment coefficient with angle of attack $(\partial C_h/\partial \alpha)$
C_{L_δ}	rate of change of lift coefficient with aileron deflection $(\partial C_L/\partial \delta_a)$
C_{m_δ}	rate of change of pitching-moment coefficient with aileron deflection $(\partial C_m/\partial \delta_a)$
$\partial C_m/\partial C_L$	rate of change of pitchimg-moment coefficient with lift coefficient
M	free-stream Mach number (V/a)

a speed of sound in free air

C_{L_α} trim-lift-curve slope

C_{l_p} damping-in-roll factor $\left(\partial C_l / \partial \frac{pb}{2V}\right)$

Subscript:

R right aileron

MODEL AND APPARATUS

A three-view drawing of the model is shown in figure 2 and the geometric characteristics are presented in table I. The model had a wing sweptback 40° at the quarter-chord line, aspect ratio 4, taper ratio 0.5, and 10-percent-thick circular-arc sections normal to the quarter-chord line. The wing was at a 3° incidence angle with respect to the fuselage center line and had 3° geometric dihedral. Measurements indicated the right-wing tip to be twisted 0.2° with respect to the left-wing tip. The fuselage and canopy coordinates are given in reference 10.

The four aileron profiles investigated (see fig. 3) included a true-contour (circular-arc) and three flat-sided ailerons having ratios of trailing-edge thickness to hinge-line thickness of 0, 0.5, and 1.0. The ailerons had chords 20 percent of the wing chord and were located on the outboard 50 percent of the wing semispans.

The model was mounted on a sting support (see fig. 4) and its angle in the horizontal plane was remotely controlled in such a manner that the model remained essentially in the center of the test section. With the model rotated 90° (wings horizontal), the angle-of-attack mechanism was used to provide angles of yaw.

The stabilizer angle could be remotely controlled by means of an electric motor mounted within the fuselage of the model. The aileron deflections were set manually.

Forces and moments on the model were measured by means of a six-component strain-gage balance housed within the model. A separate strain-gage balance was mounted on the right aileron for the determination of the aileron hinge moments.

The tests were conducted in the Langley 4- by 4-foot supersonic tunnel which is described in reference 10.

TESTS

Test Conditions

The test conditions are summarized in the following table:

Mach number	Stagnation pressure (atm)	Stagnation temperature ($^{\circ}$F)	Dewpoint ($^{\circ}$F)	Dynamic pressure (lb/sq ft)	Reynolds number (based on $\bar{c}$)
1.59	0.25	110	-35	223	575,000
1.40	.25	110	-30	229	600,000

Calibration data for the Mach number 1.59 nozzle are presented in reference 10 and for the Mach number 1.40 nozzle in reference 11.

Corrections and Accuracy

No corrections due to sting interference were applied to the data. The exact magnitude of the sting effects is not known though it is believed to be small (see reference 12).

Base-pressure measurements at a Mach number of 1.59 indicated that, if free-stream static pressure is assumed to exist at the base of the model, then the drag data presented would be reduced by approximately 1 percent in the angle-of-attack range from 4° to 10°, with no correction necessary in the lower angle range.

Optical measurements of the wing twist under load ($\delta_a = 0$) indicated twists of less than 0.05° and hence no corrections for aeroelastic effects were made. No measurements were made of the wing twist with the aileron deflected.

The maximum uncertainties in the aerodynamic coefficients are of the order indicated in the following table:

Coefficient	Random balance-system errors	Balance-system and tunnel errors combined
C_L	±0.0010	±0.0043
C_D	±.00025	±.0023
C_Y	±.0010	±.0019
C_m	±.00045	±.0014
C_n	±.00011	±.00015
C_l	±.00006	±.000099
C_h	±.0028	±.0031

A more complete analysis of the balance-system accuracy is presented in reference 13.

The accuracy of the angle of attack was about ±0.05°, the tail incidence about ±0.10°, the aileron deflection about ±0.05°, and the dynamic pressure about 0.25 percent.

Because of the small magnitude of the flow gradients in the vicinity of the model (references 10 and 11), no corrections for these effects have been made. Tests of the model in the horizontal and vertical planes showed good agreement.

Test Procedure

All four aileron profiles were investigated at $M = 1.59$ but only the circular-arc and $t = 0.5$ profiles were investigated at $M = 1.40$. The aileron tests covered an angle-of-attack range from -4° to 10° with aileron deflections from -15° to 15° with the exception of the circular-arc profile at $M = 1.40$ where only positive deflections were tested. The right aileron only was deflected for all tests with the left aileron fixed at zero deflection.

In addition, tests were made through an angle-of-yaw range from -10° to 10° at $\alpha = 0°$ and $M = 1.59$ for the model equipped with each of the flat-sided ailerons ($\delta_a = 0°$).

RESULTS AND DISCUSSION

Presentation of Data

The aerodynamic characteristics in pitch for the model with various aileron profiles at $\delta_a = 0^\circ$ are given in figures 5 and 6 for Mach numbers of 1.59 and 1.40, respectively. The variation of the lift, drag, and pitching-moment coefficients with aileron deflection at the angle of attack for zero lift is presented in figure 7.

The effects of the three flat-sided ailerons on the lateral characteristics in yaw for the model at $\alpha = 0^\circ$ and $\delta_a = 0^\circ$ are presented in figure 8 for $M = 1.59$.

The effect of aileron deflection on the rolling-moment, yawing-moment, and aileron hinge-moment coefficients through an angle-of-attack range for the various profiles is given in figures 9 and 10 for $M = 1.59$ and 1.40, respectively. The variation of the rolling-moment and aileron hinge-moment coefficients with aileron deflection at the angle of attack for zero lift is presented in figure 11. The effects of profile on the rolling effectiveness $\frac{pb/2V}{\delta_a}$ through a Mach number range as obtained from various sources are presented in figure 12.

Some of the pertinent aerodynamic characteristics are presented as a function of trailing-edge angle in figure 13. The selection of the trailing-edge angle as a basis of comparison may be somewhat hypothetical inasmuch as the direct effects of the trailing-edge angle, the aileron thickness, and the aileron-surface curvature cannot be isolated. In this figure, a faired line is shown for the $M = 1.59$ results but, since only two profiles were tested at $M = 1.40$, only the points are shown. The faired line is solid from the $t = 1.0$ profile to the $t = 0$ profile since these ailerons had flat sides and represented systematic increases in trailing-edge angle and decreases in profile thickness. The line between the $t = 0$ aileron and the circular-arc aileron is dashed since this change results in an increase in trailing-edge angle as well as an increase in profile-thickness distribution. The slopes presented in figure 13 were obtained at the angle of attack for zero lift.

The variation of C_{l_δ} and C_{h_δ} with angle of attack for both Mach numbers is shown in figure 14 together with the theoretical estimates. A comparison between the experimental and theoretical values of C_{L_δ}, C_{l_δ}, C_{h_δ} as a function of trailing-edge angle is shown in figure 15. The theoretical values presented on these figures were obtained by

determining the linear three-dimensional control-surface characteristics by the method of reference 14 and then applying a thickness correction factor. (See table II.) The correction factors at $M = 1.59$ for all except the $t = 1.0$ profile were obtained by the use of reference 15 and were applied in the same manner as that used in reference 6. This procedure involves the assumption that the thickness effects on the aileron characteristics are the same for the conical-flow regions as for the two-dimensional-flow regions. In addition, the theory of reference 15 is limited to conditions where the leading-edge shock wave is attached, whereas for the present model the leading-edge shock wave is detached at both Mach numbers and for all angles of attack. The presence of this detached shock was neglected in the theoretical calculations. The method of reference 15 is not considered applicable for Mach number components normal to the control-surface leading edge of less than 1.3 or for profiles having parallel sides. For these conditions ($M = 1.40$ and $t = 1.0$ profile) it was arbitrarily assumed that local sonic velocity occurred very near the leading edge of the wing and the calculations for the correction factors were obtained by means of the oblique-shock equations and the isentropic expansion and compression equations. The assumption that local sonic velocity occurred near the leading edge appears reasonable since, because of the detached shock, a region of subsonic flow exists just ahead of the leading edge that must accelerate to a low supersonic velocity as it passes over the airfoil nose. This effect was noted in connection with the wing-pressure measurements presented in reference 16.

Longitudinal Characteristics

The basic longitudinal data for the model with the various aileron profiles at $\delta_a = 0^\circ$ (figs. 5 and 6) show no unusual trends.

The variation of lift, drag, and pitching-moment coefficients with aileron deflection (fig. 7) was obtained by cross-plotting from the basic data for the various aileron deflections at the angle of attack for zero lift (approximately -2.4° for each configuration). In the case of pitching moments, the curves were shifted to show $C_m = 0$ at $\delta_a = 0^\circ$ so that the results for the various profiles might be more readily compared. The lift, drag, and pitching-moment trends indicated in figure 7 apply to the complete model with both ailerons deflected in the same direction in the manner of longitudinal-control devices.

In general, the variations of the lift and pitching-moment coefficients with aileron deflection are fairly linear, especially through the deflection range of about $\pm 6^\circ$. The circular-arc and $t = 0$ profiles appear to be relatively ineffective in producing lift or pitching moment. In particular, the lift effectiveness of the circular-arc-profile aileron is quite low at $M = 1.40$ and is about zero at $M = 1.59$. This

[redacted]

ineffectiveness might be expected inasmuch as pressure measurements of the wing with circular-arc sections (reference 16 for $M = 1.59$ and unpublished results for $M = 1.40$) indicate separation to exist over the outboard, trailing-edge section of the wing. Increasing the thickness of the aileron trailing edge ($t = 0.5$ and $t = 1.0$ profiles) resulted in slightly higher lift and pitching-moment effectiveness. The lift and pitching-moment effectiveness for each profile was constant through the angle-of-attack range investigated.

There is an increase in the drag coefficients with aileron deflection that is slightly greater for positive deflections and for the ailerons with thickened trailing edges.

The summary of the longitudinal characteristics as a function of the trailing-edge angle (fig. 13) shows little change in the lift-curve slope or the drag. There is a general trend toward higher lift and pitch effectiveness and higher static longitudinal stability as the trailing-edge angle is decreased. This higher effectiveness and stability probably results from a lessening of the separation effects over the outboard trailing-edge section of the wing.

Lateral Characteristics

The effects of aileron profile on the lateral characteristics in yaw (fig. 8) are small with the possible exception of the rolling-moment variation where the ailerons with thickened trailing edges indicate greater rolling moments due to yaw. This effect might be expected as a result of improved flow conditions over the outboard section of the wing.

Aileron-Control Characteristics

The variation of the rolling-moment and hinge-moment coefficients with angle of attack (figs. 9 and 10) is slightly nonlinear for the circular-arc and $t = 0$ profiles, particularly for the negative deflections. This condition is probably a result of the separation effects, which, as already pointed out, occur over the rear section of the circular-arc airfoil and probably occur over the $t = 0$ profile. The nonlinearity of the hinge-moment curves for small angles of attack and small deflection angles is similar to the low-speed characteristics of ailerons having large trailing-edge angles (reference 17). The slope of the curve of hinge-moment coefficient against angle of attack $\left(C_{h_\alpha}\right)$ for the circular-arc and $t = 0$ profiles reverses in the region near zero lift ($\alpha \approx -2.4^\circ$, $\delta_a = 0^\circ$). A tendency toward reduced aileron effectiveness for the small deflections is also evident near zero lift.

The effect of reducing the trailing-edge angle by increasing the trailing-edge thickness of the aileron to 0.5 and 1.0 times the hinge-line thickness was to eliminate the nonlinearity of the rolling-moment and hinge-moment curves and to eliminate the tendency toward roll reversal at small angles of attack and small deflections.

The negative rolling moments occurring for $\delta_a = 0^\circ$ at $M = 1.40$ (fig. 10) can be attributed to the slight twist of the wing. At $M = 1.59$ (fig. 9) the effects of the twist appear to be counteracted by flow angularities in the region of the wing tips.

The adverse yawing moment produced by aileron deflection (figs. 9 and 10) is about the same as that obtained at low speeds for a similar configuration (reference 9). Changes in the aileron profile had little effect on the adverse yaw.

The variation of the rolling-moment and hinge-moment coefficients with aileron deflection at the angle of attack for zero lift is presented in figure 11. As a consequence of the asymmetry indicated for the $M = 1.40$ data, the results presented in figure 11 for this Mach number have been shifted to show $C_l = 0$ and $C_h = 0$ at $\delta_a = 0^\circ$. The results on this figure apply to the complete model with only the right aileron deflected.

The nonlinearity of the rolling-moment and hinge-moment coefficients for small aileron deflections for the circular-arc and $t = 0$ profiles is apparent in figure 11. From an examination of figures 9, 10, and 14, it can be seen that the nonlinearity for small deflections disappears for angles of attack above about 4° and the variations of rolling-moment and hinge-moment coefficients with aileron deflection C_{l_δ} and C_{h_δ} become about constant and are slightly higher than the values near zero lift. As the positive angle of attack is increased, however, the regions of nonlinearity in the curves of rolling moment and hinge moment tend to shift toward the higher negative deflections (see fig. 9). Similar variations in both C_{l_δ} and C_{h_δ} are indicated for the circular-arc and $t = 0$ profiles. Changing the profile to $t = 0.5$ and $t = 1.0$ removed the nonlinearity at small deflections and increased the values of both C_{l_δ} and C_{h_δ}. The $t = 1.0$ profile showed only slight improvement over that shown by the $t = 0.5$ profile.

The results near zero lift are summarized in figure 13 where C_{l_δ}, C_{h_δ}, and C_{h_α} are presented as a function of the trailing-edge angle. Similar trends are indicated for the two Mach numbers although each of the parameters have higher values at $M = 1.40$.

The rolling effectiveness $\frac{pb/2V}{\delta_a}$ for the various profiles is presented in figure 12 for a Mach number range up to 1.90. The low-speed value (M = 0.16) was obtained from reference 9 by using a value for the damping in roll C_{l_p} obtained from reference 18. The transonic results (faired lines) were obtained from free-flight tests of rolling rocket models (reference 4). The results at M = 1.40 and 1.59 were obtained from the present tests and those at M = 1.90 were obtained from reference 7, in each case, by using values of C_{l_p} obtained from charts presented in reference 19. None of the tunnel results was corrected to account for the effects of adverse yaw or wing twist that may occur on a free-rolling wing.

The variation of $\frac{pb/2V}{\delta_a}$ with Mach number (fig. 12) indicates a large reduction in effectiveness beginning at a Mach number of about 0.8. The results of the rocket-model tests show the reversal obtained for the circular-arc profile near M = 0.95 and the improvement obtained with the t = 0.5 and t = 1.0 profile.

Comparison with Theory

The values of C_{l_δ} and C_{h_δ} obtained experimentally are, in general, somewhat lower than those obtained theoretically (fig. 14). This result might be expected inasmuch as the theoretical values neglect the boundary-layer and separation effects as well as any detached shock effects. The effects of separation on the aileron characteristics may be influenced by the Reynolds number although the results of an investigation of a 63° sweptback wing (reference 20) indicated little effect of Reynolds number on the characteristics of an outboard trailing-edge flap. The variation of the theoretical values of C_{l_δ}, C_{h_δ}, and C_{L_δ} with trailing-edge angle (fig. 15) is similar to that shown by the experimental values and indicates that the thickness correction factors are reasonable. The experimental and theoretical values of C_{L_δ} are in good agreement although the experimental values of aileron effectiveness C_{l_δ} are somewhat lower than the theoretical values. This effect might also be attributed to separation near the tip which would result in the aileron center of lift being farther inboard than predicted by theory.

CONCLUSIONS

The results of the investigation conducted at Mach numbers of 1.40 and 1.59 to determine the effects of aileron profile on the aerodynamic

characteristics of a complete model of a supersonic aircraft configuration indicated low aileron effectiveness for the circular-arc-profile aileron and the flat-sided aileron having a ratio of trailing-edge thickness to hinge-line thickness t of 0. Increasing the trailing-edge thickness of the aileron ($t = 0.5$ and 1.0) resulted in increased aileron effectiveness and higher aileron hinge moments with only a slight increase in drag.

The aileron lift effectiveness C_{L_δ} was in reasonably good agreement with theory although the variations of rolling- and hinge-moment coefficients with aileron deflection, C_{l_δ} and C_{h_δ}, were, in general, somewhat less than that predicted by theory. The variation of C_{l_δ}, C_{h_δ}, and C_{L_δ} with trailing-edge angle for the various aileron profiles agreed well with the theoretical results.

Langley Aeronautical Laboratory
National Advisory Committee for Aeronautics
Langley Field, Va.

REFERENCES

1. Sandahl, Carl A.: Free-Flight Investigation at Transonic and Supersonic Speeds of the Rolling Effectiveness of a 42.7° Swept-back Wing Having Partial-Span Ailerons. NACA RM L8E25, 1948.

2. Turner, Thomas R., Lockwood, Vernard E., and Vogler, Raymond D.: Preliminary Investigation of Various Ailerons on a 42° Sweptback Wing for Lateral Control at Transonic Speeds. NACA RM L8D21, 1948.

3. Turner, Thomas R., Lockwood, Vernard E., and Vogler, Raymond D.: Aerodynamic Characteristics at Subsonic and Transonic Speeds of a 42.7° Sweptback Wing Model Having an Aileron with Finite Trailing-Edge Thickness. NACA RM L8K02, 1949.

4. Sandahl, Carl A.: Free-Flight Investigations at Transonic and Supersonic Speeds of the Rolling Effectiveness of Several Aileron Configurations on a Tapered Wing Having 42.7° Sweepback. NACA RM L8K23, 1949.

5. Sivells, James C., and Conner, D. William: Preliminary Investigation at a Mach Number of 1.9 and a Reynolds Number of 2,200,000 of Three Ailerons Applicable to the Bell XS-2 Airplane Design. NACA RM L8D02, 1948.

6. Sivells, James C., and Goin, Kennith L.: Experimental and Calculated Hinge Moments of Two Ailerons on a 42.7° Sweptback Wing at a Mach Number of 1.9. NACA RM L8K24a, 1949.

7. Goin, Kennith L.: Investigation at a Mach Number of 1.9 and a Reynolds Number of 2.2×10^6 of Several Flap-Type Lateral-Control Devices on a Wing Having 42.7° Sweepback of the Leading Edge. NACA RM L9A18a, 1949.

8. Lockwood, Vernard E.: Damping-in-Roll Characteristics of a 42.7° Sweptback Wing as Determined from a Wind-Tunnel Investigation of a Twisted Semispan Wing. NACA RM L9F15, 1949.

9. Goodson, Kenneth W., and Comisarow, Paul: Lateral Stability and Control Characteristics of an Airplane Model Having a 42.8° Sweptback Circular-Arc Wing with Aspect Ratio 4.00, Taper Ratio 0.50, and Sweptback Tail Surfaces. NACA RM L7G31, 1947.

10. Cooper, Morton, Smith, Norman F., and Kainer, Julian H.: A Pressure-Distribution Investigation of a Supersonic Aircraft Fuselage and Calibration of the Mach Number 1.59 Nozzle of the Langley 4- by 4-Foot Supersonic Tunnel. NACA RM L9E27a, 1949.

11. Hasel, Lowell E., and Sinclair, Archibald R.: A Pressure-Distribution Investigation of a Supersonic-Aircraft Fuselage and Calibration of the Mach Number 1.40 Nozzle of the Langley 4- by 4-Foot Supersonic Tunnel. NACA RM L50B14a, 1950.

12. Osborne, Robert S.: High-Speed Wind-Tunnel Investigation of the Longitudinal Stability and Control Characteristics of a $\frac{1}{16}$-Scale Model of the D-558-2 Research Airplane at High Subsonic Mach Numbers and at a Mach Number of 1.2. NACA RM L9C04, 1949.

13. Robinson, Ross B.: An Investigation of a Supersonic Aircraft Configuration Having a Tapered Wing with Circular-Arc Sections and 40° Sweepback. Static Lateral Control Characteristics at Mach Numbers of 1.40 and 1.59. NACA RM L50I11, 1950.

14. Kainer, Julian H., and Marte, Jack E.: Theoretical Supersonic Characteristics of Inboard Trailing-Edge Flaps Having Arbitrary Sweep and Taper. Mach Lines behind Flap Leading and Trailing Edges. NACA TN 2205, 1950.

15. Morrissette, Robert R., and Oborny, Lester F.: Theoretical Characteristics of Two-Dimensional Supersonic Control Surfaces. NACA RM L8G12, 1948.

16. Cooper, Morton, and Spearman, M. Leroy: An Investigation of a Supersonic Aircraft Configuration Having a Tapered Wing with Circular-Arc Sections and 40° Sweepback. A Pressure-Distribution Study of the Aerodynamic Characteristics of the Wing at Mach Number 1.59. NACA RM L50C24, 1950.

17. Langley Research Department (Compiled by Thomas A. Toll): Summary of Lateral-Control Research. NACA Rep. 868, 1947.

18. Toll, Thomas A., and Queijo, M. J.: Approximate Relations and Charts for Low-Speed Stability Derivatives of Swept Wings. NACA TN 1581, 1948.

19. Harmon, Sidney M., and Jeffreys, Isabella: Theoretical Lift and Damping in Roll of Thin Wings with Arbitrary Sweep and Taper at Supersonic Speeds. Supersonic Leading and Trailing Edges. NACA TN 2114, 1950.

20. Olson, Robert N., and Mead, Merrill H.: Aerodynamic Study of a Wing-Fuselage Combination Employing a Wing Swept Back 63°. Effectiveness of an Elevon as a Longitudinal Control and the Effects of Camber and Twist on the Maximum Lift-Drag Ratio at Supersonic Speeds. NACA RM A50A31a, 1950.

TABLE I

GEOMETRIC CHARACTERISTICS OF MODEL

Wing:	
Area, sq ft	1.158
Span, ft	2.155
Aspect ratio	4
Sweepback of quarter-chord line, deg	40
Taper ratio	0.5
Mean aerodynamic chord, ft	0.557
Airfoil section normal to quarter-chord line	10-percent-thick, circular-arc
Twist, deg	0
Dihedral, deg	3
Incidence, deg	3
Horizontal tail:	
Area, sq ft	0.196
Span, ft	0.855
Aspect ratio	3.72
Sweepback of quarter-chord line, deg	40
Taper ratio	0.5
Airfoil section	NACA 65-008
Vertical tail:	
Area (exposed), sq ft	0.172
Aspect ratio (based on exposed area and span)	1.17
Sweepback of leading edge, deg	40.6
Taper ratio	0.337
Airfoil section, root	NACA 27-010
Airfoil section, tip	NACA 27-008
Fuselage:	
Fineness ratio (neglecting canopies)	9.4
Miscellaneous:	
Tail length from $\bar{c}/4$ wing to $\bar{c}_t/4$ tail, ft	0.917
Tail height, wing semispans above fuselage center line	0.153

TABLE II

THEORETICAL CONTROL-SURFACE CHARACTERISTICS

(a) M = 1.40.

Profile / Condition	Circular arc			t = 0			t = 0.5			t = 1.0		
	C_{h_δ}	C_{l_δ}	C_{L_δ}	C_{h_δ}	C_{l_δ}	C_{L_δ}	C_{h_δ}	C_{l_δ}	C_{L_δ}	C_{h_δ}	C_{l_δ}	C_{L_δ}
Linear theory	-0.0320	-0.0014	0.0036	-0.0320	-0.0014	0.0036	-0.0320	-0.0014	0.0036	-0.0320	-0.0014	0.0036
Correction factor	.382	.394	.394	.403	.403	.403	.464	.464	.464	.569	.569	.569
Corrected solution	-.0122	-.00055	.0014	-.0129	-.00056	.0015	-.0149	-.00065	.0017	-.0182	-.00080	.002

(b) M = 1.59.

Profile / Condition	Circular arc			t = 0			t = 0.5			t = 1.0		
	C_{h_δ}	C_{l_δ}	C_{L_δ}	C_{h_δ}	C_{l_δ}	C_{L_δ}	C_{h_δ}	C_{l_δ}	C_{L_δ}	C_{h_δ}	C_{l_δ}	C_{L_δ}
Linear theory	-0.0227	-0.00097	0.0026	-0.0227	-0.00097	0.0026	-0.0227	-0.00097	0.0026	-0.0227	-0.00097	0.0026
Correction factor	.428	.478	.478	.477	.477	.477	.74	.74	.74	.816	.816	.816
Corrected solution	-.0097	-.00046	.0012	-.0108	-.00046	.0012	-0.0168	-.00072	.0019	-.0186	-.00079	.0021

NACA

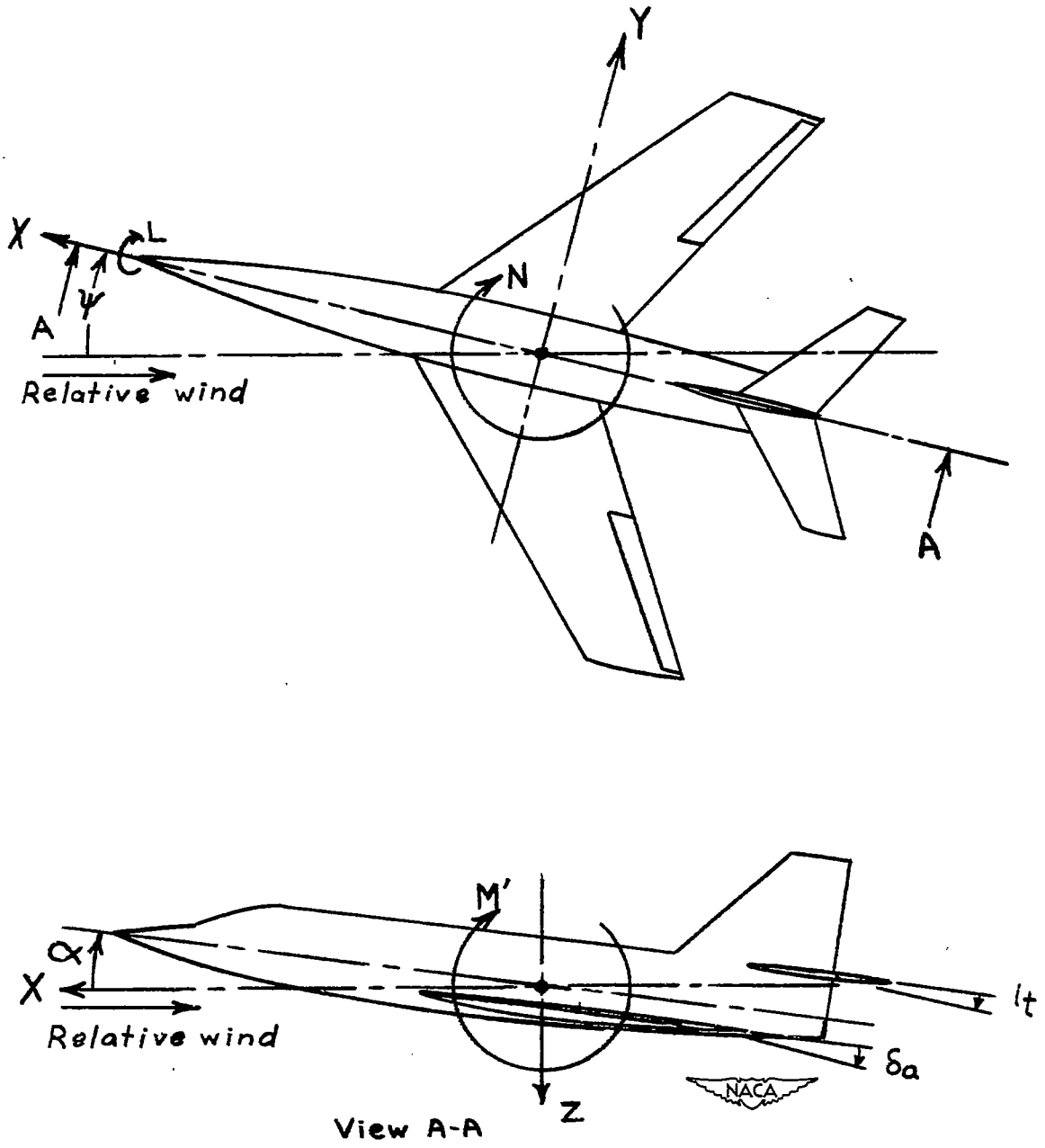

Figure 1.- System of stability axes. Arrows indicate positive values.

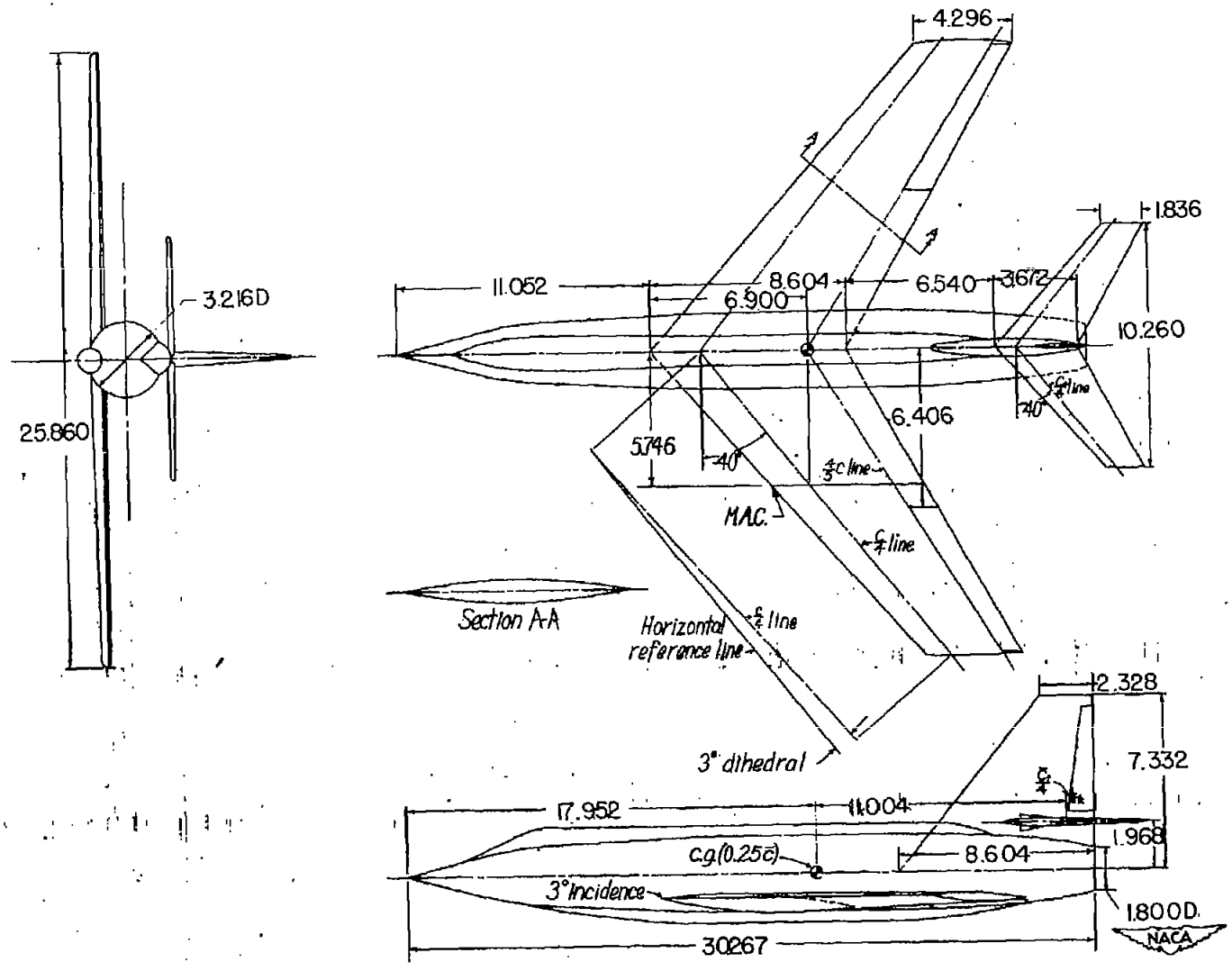

Figure 2.- Details of model of supersonic aircraft configuration. Dimensions are in inches unless otherwise noted.

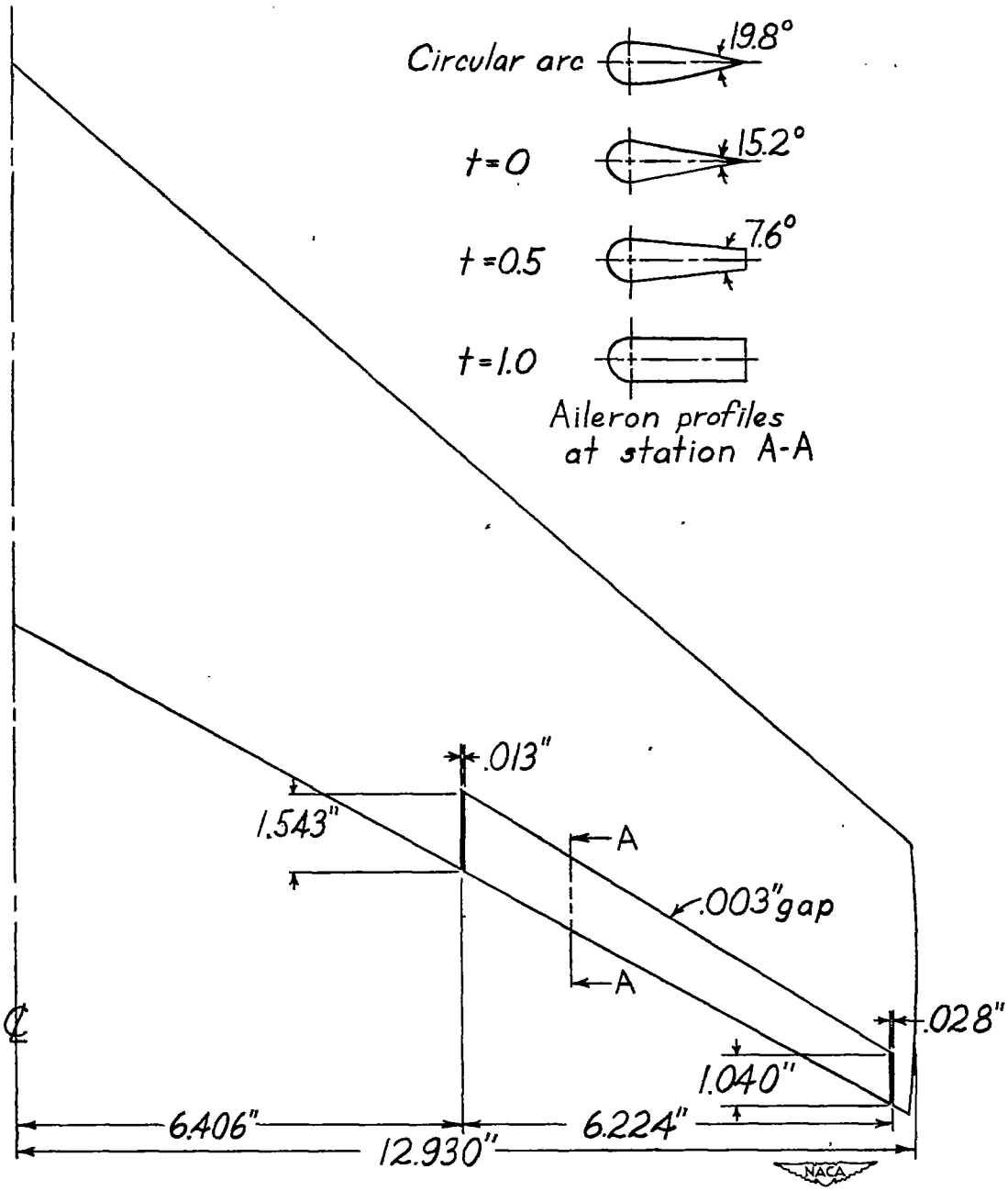

Figure 3.- Details of aileron installation.

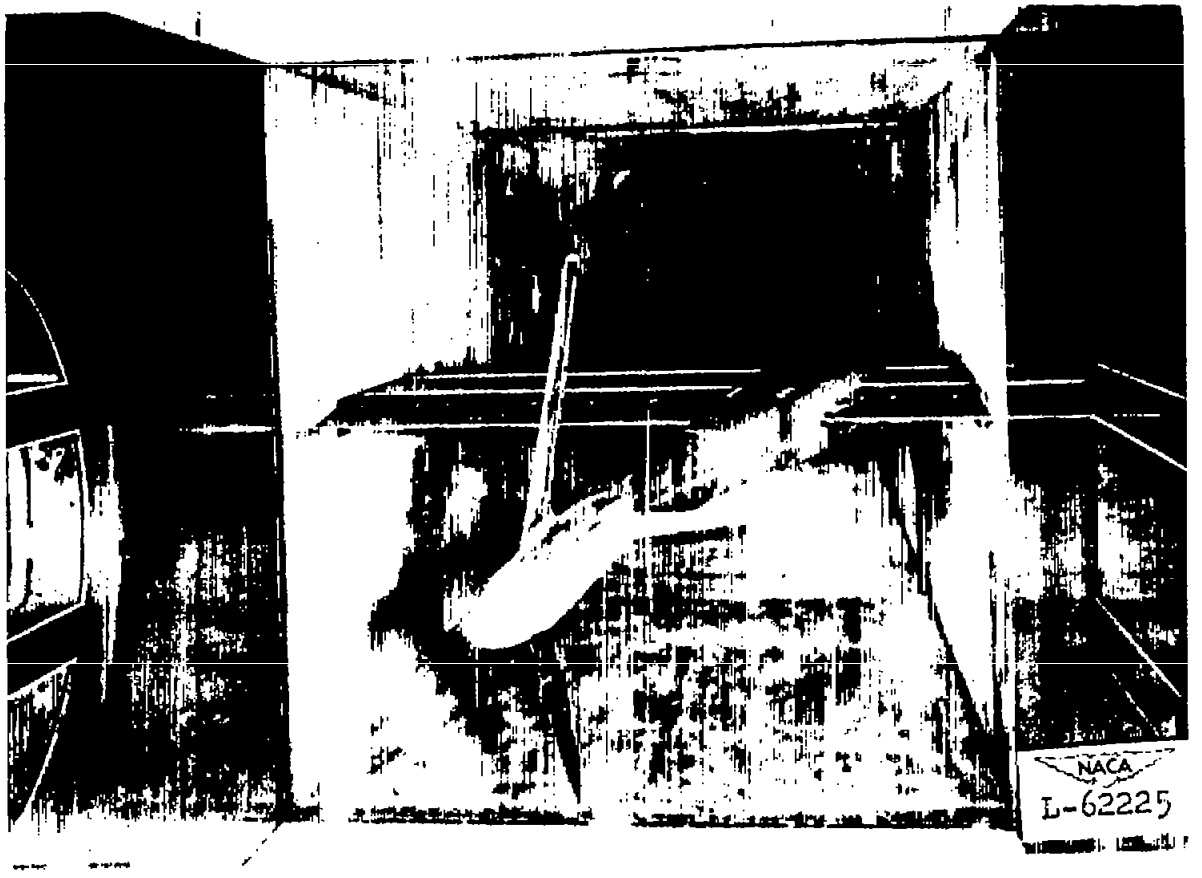

(a) Mounted for pitch tests. $\alpha = -10^{\circ}$; $\psi = 0^{\circ}$.

Figure 4.- Complete model of aircraft mounted in the Langley 4- by 4-foot supersonic tunnel.

(b) Mounted for yaw tests. $\alpha = 0^{\circ}$; $\psi = 0^{\circ}$.

Figure 4.- Concluded.

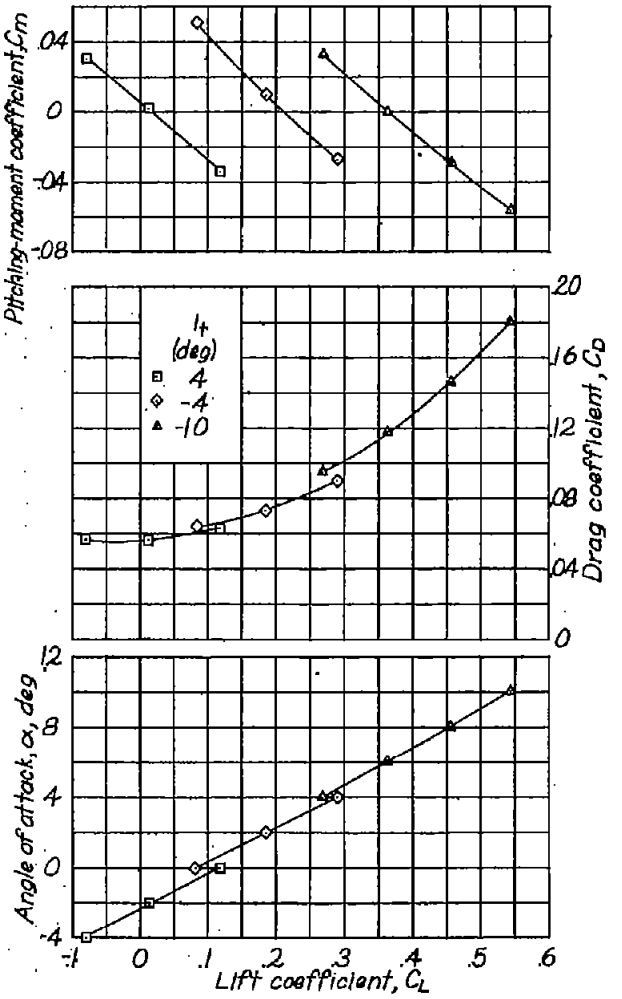

(a) Circular arc.

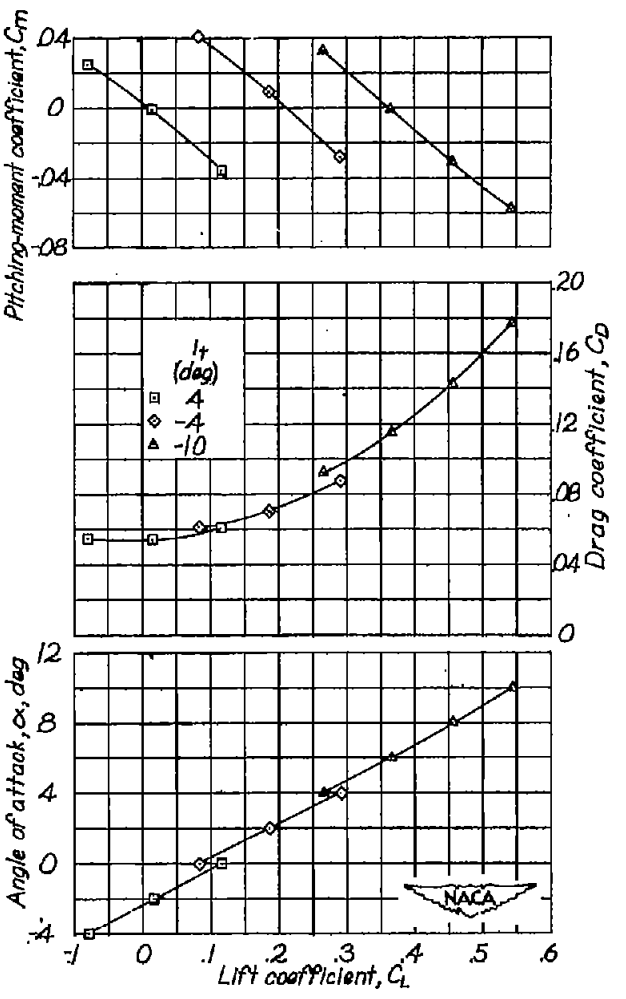

(b) t = 0.

Figure 5.- Aerodynamic characteristics in pitch for model with various aileron profiles. $\delta_a = 0^\circ$; M = 1.59.

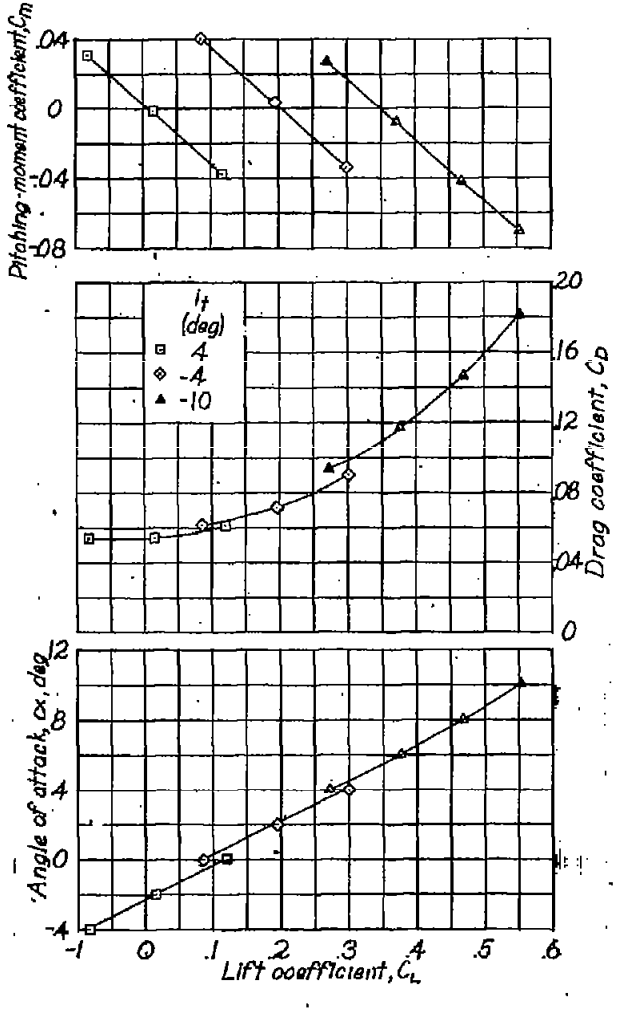

(c) t = 0.5.

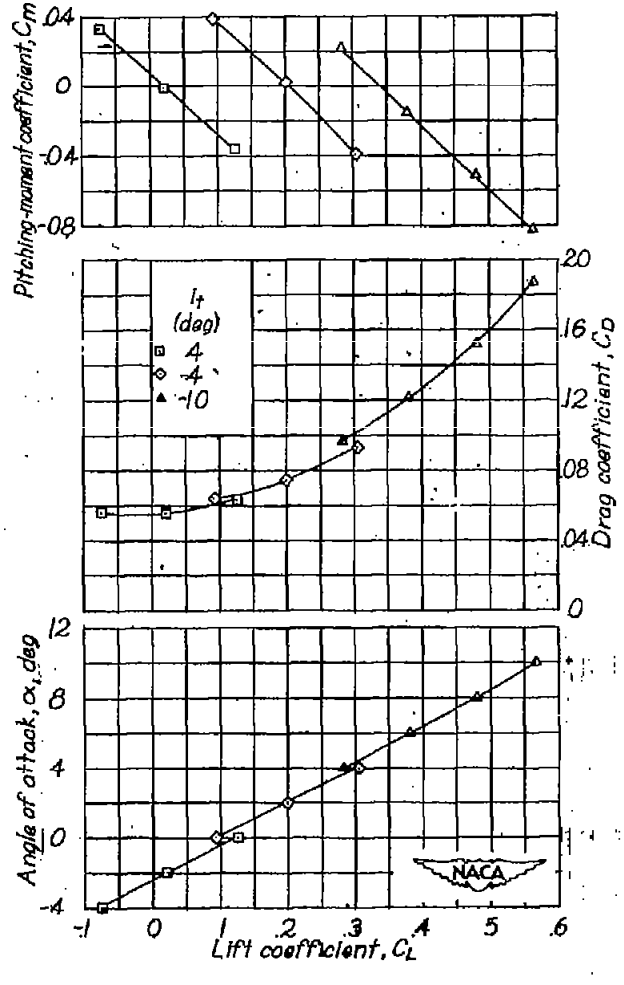

(d) t = 1.0.

Figure 5.- Concluded.

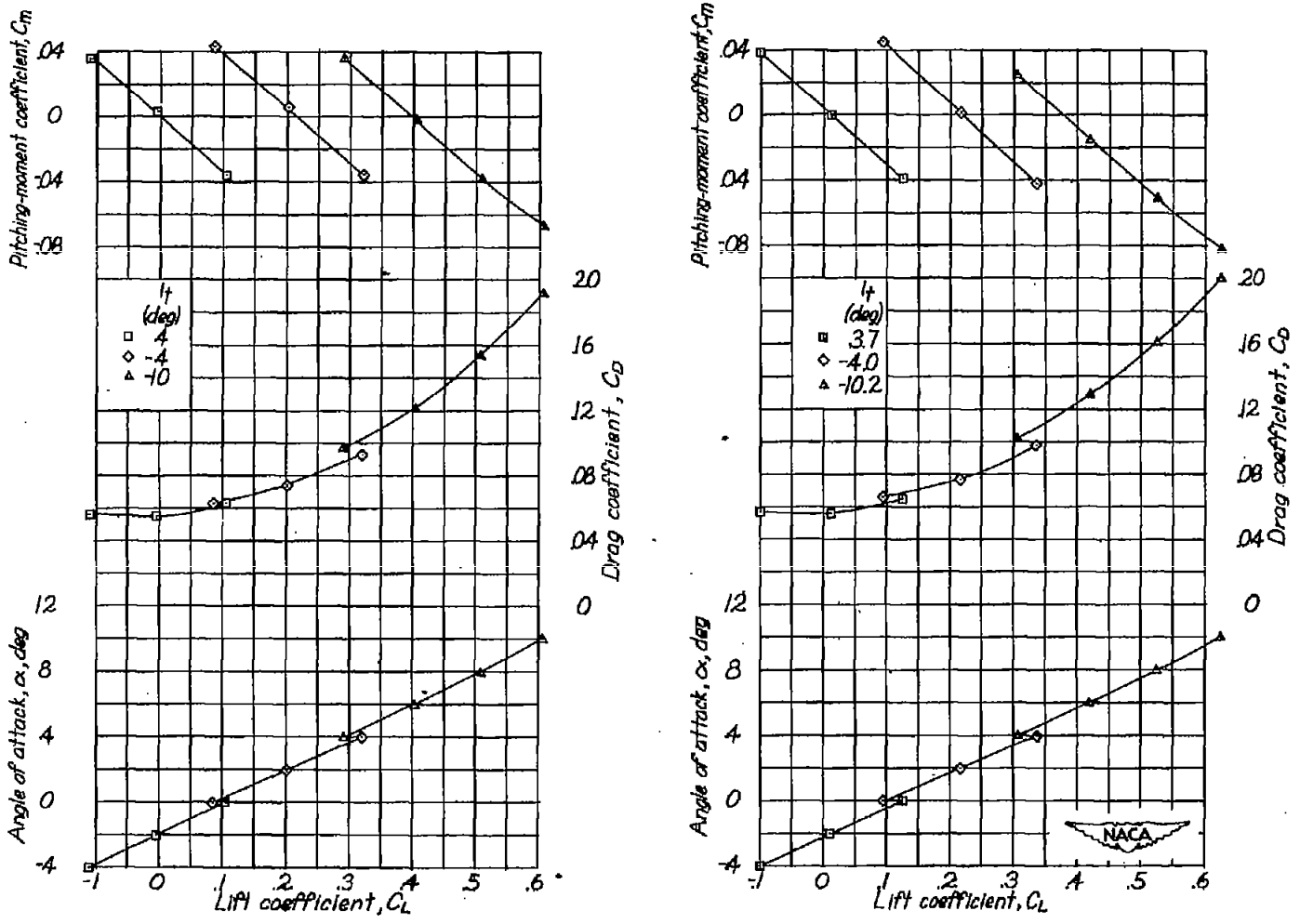

(a) Circular arc.

(b) t = 0.5.

Figure 6.- Aerodynamic characteristics in pitch for model with various aileron profiles. $\delta_a = 0^o$; M = 1.40.

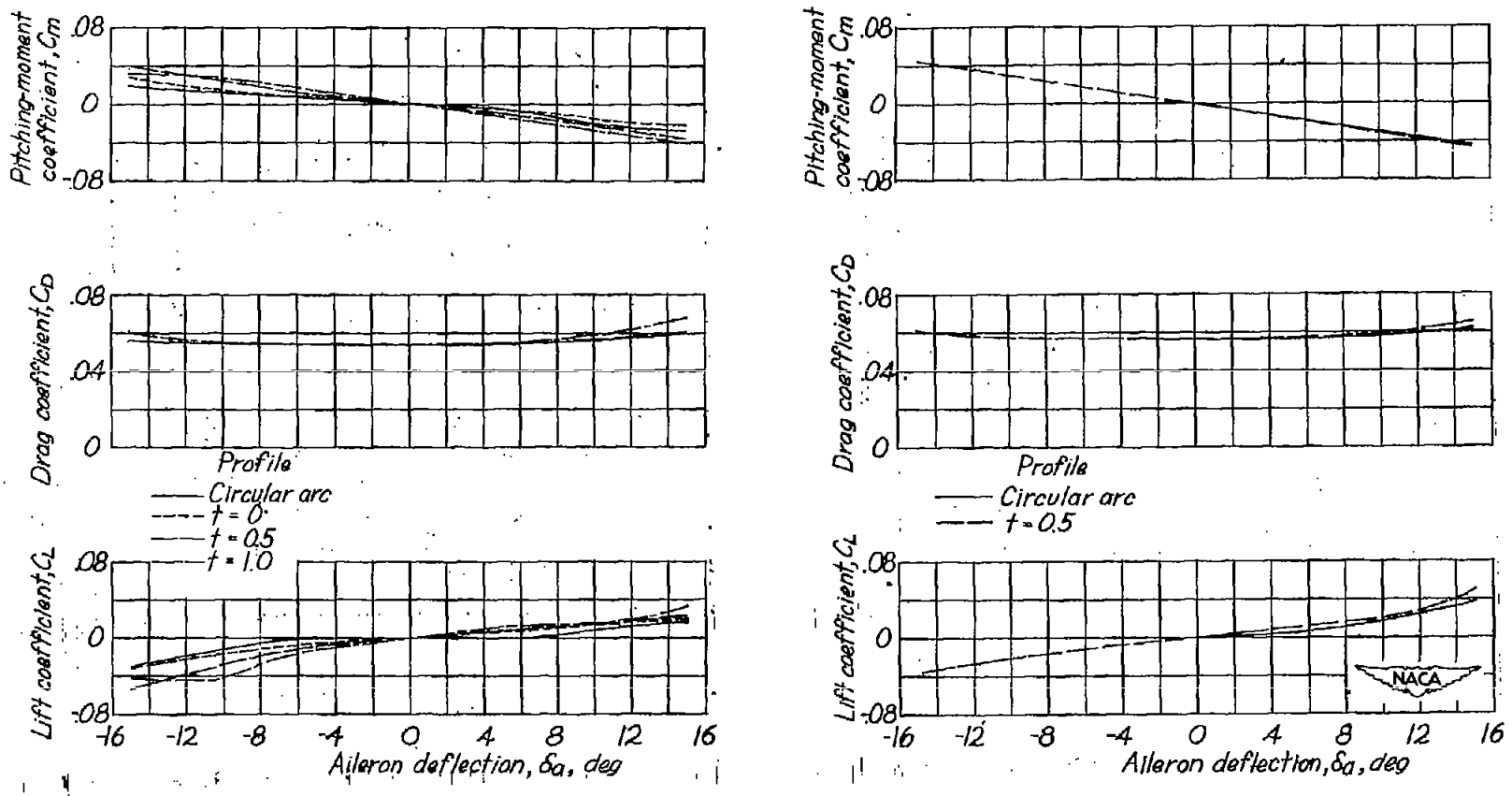

(a) M = 1.59. (b) M = 1.40.

Figure 7.- Effect of aileron deflection on the aerodynamic characteristics in pitch for the model equipped with various aileron profiles. $\alpha \approx -2.4^{\circ}$.

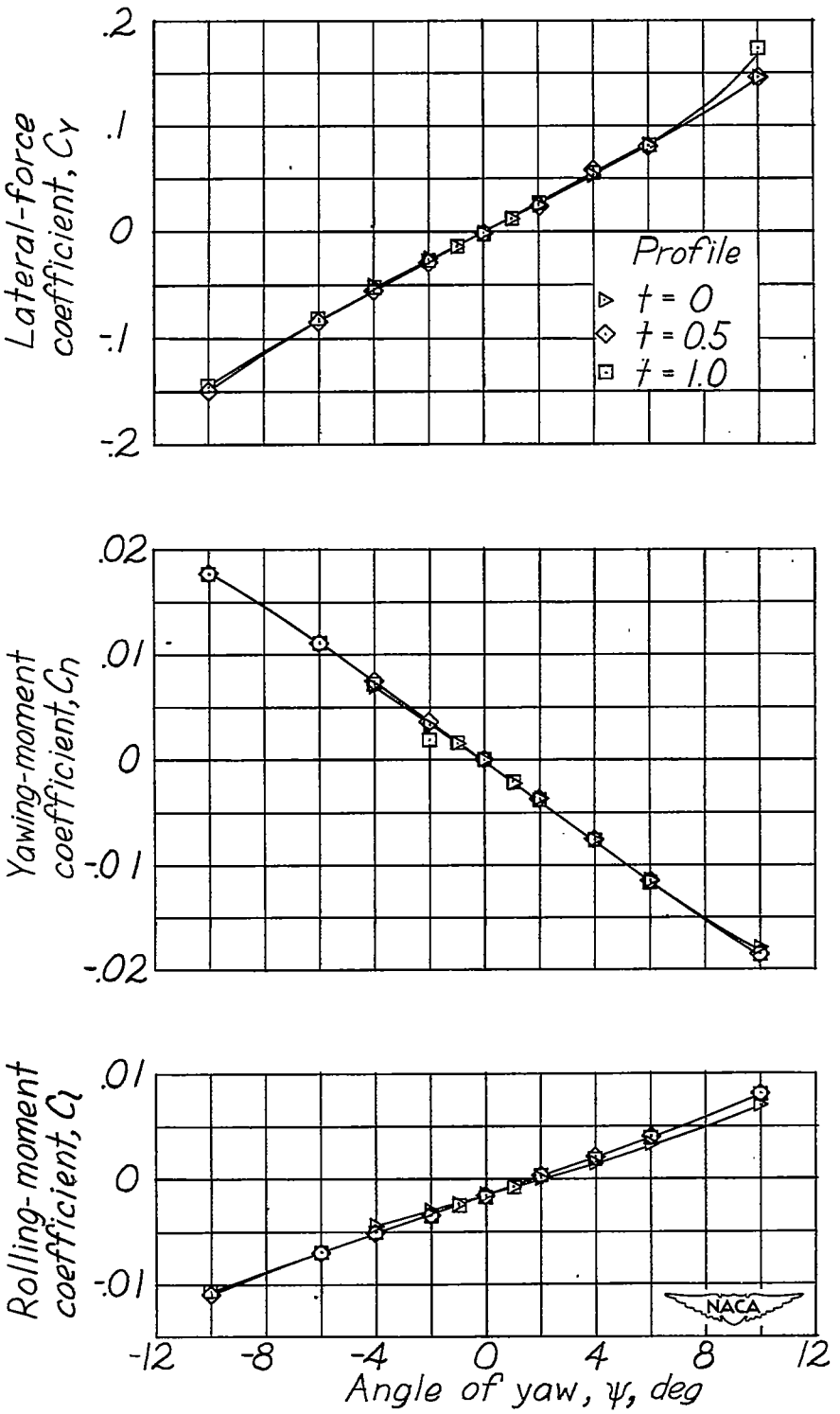

Figure 8.- Effect of aileron profile on the lateral characteristics in yaw. $\alpha = 0^\circ$; $\delta_R = 0^\circ$; M = 1.59.

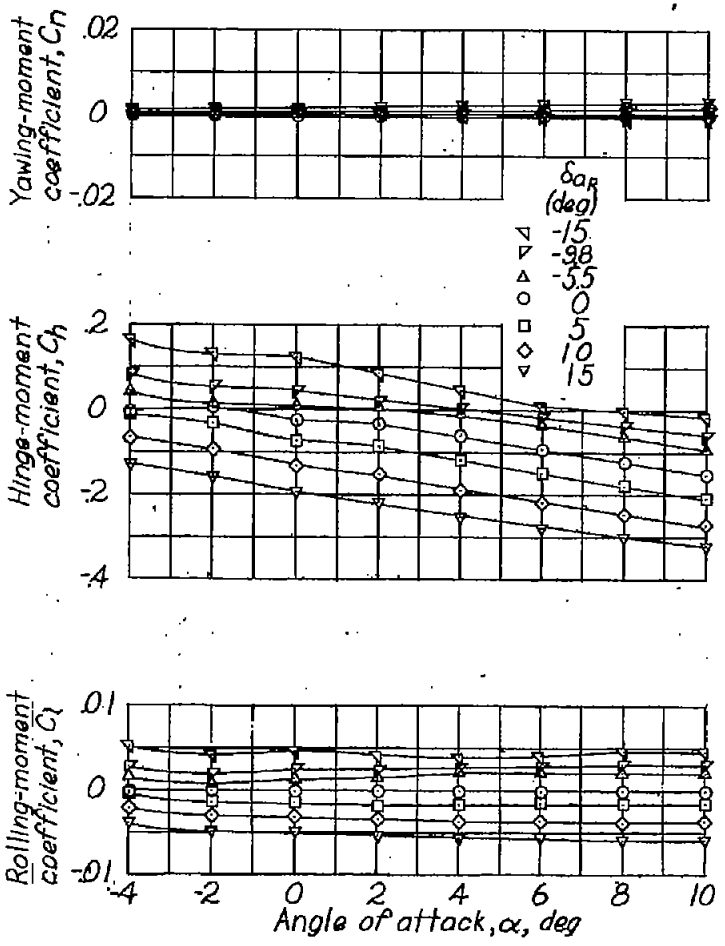

(a) Circular arc.

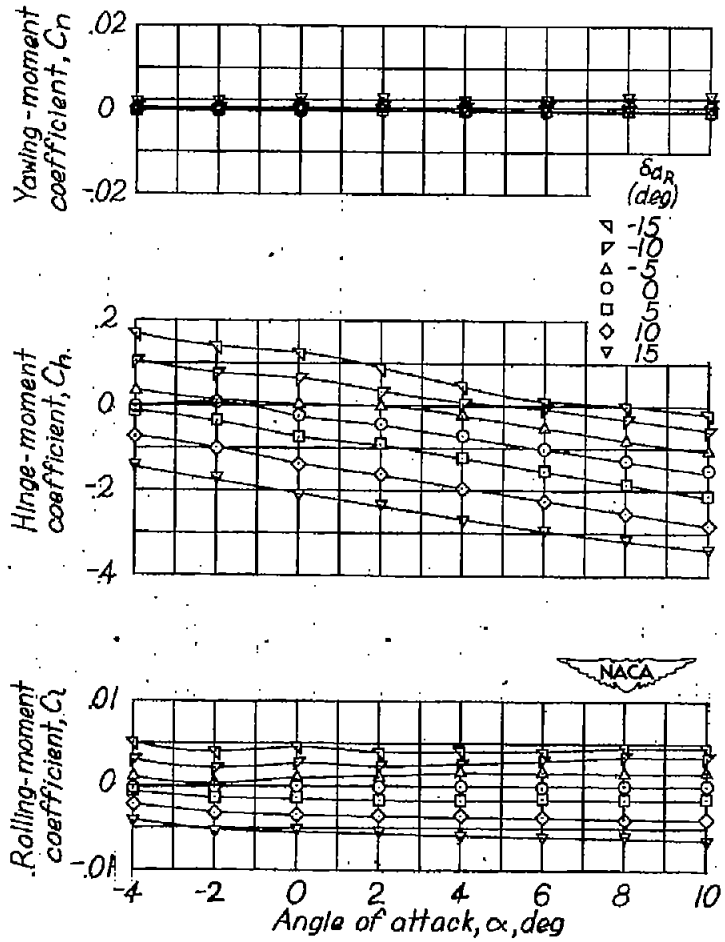

(b) t = 0.

Figure 9.- Effect of aileron deflection on the characteristics of a complete model equipped with various ailerons. M = 1.59.

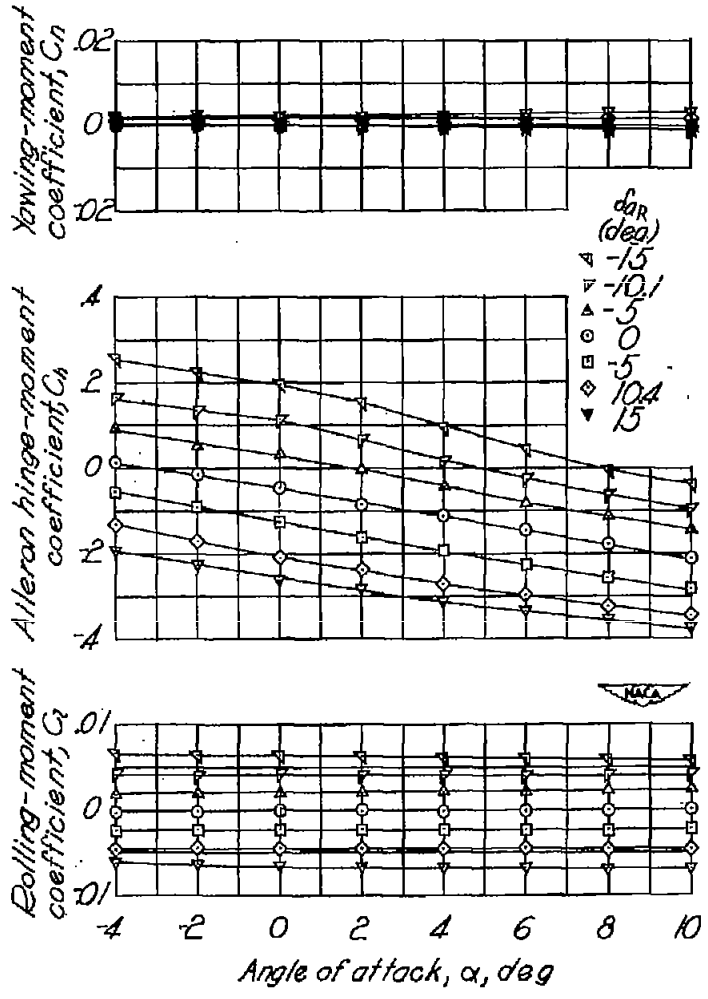

(c) t = 0.5.

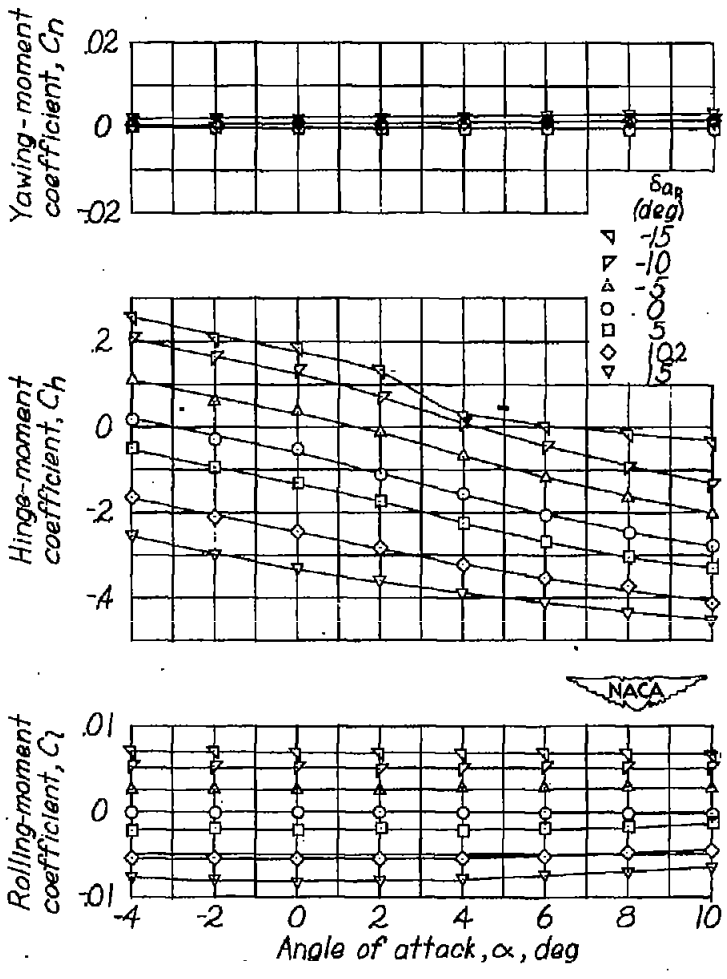

(d) t = 1.0.

Figure 9.- Concluded.

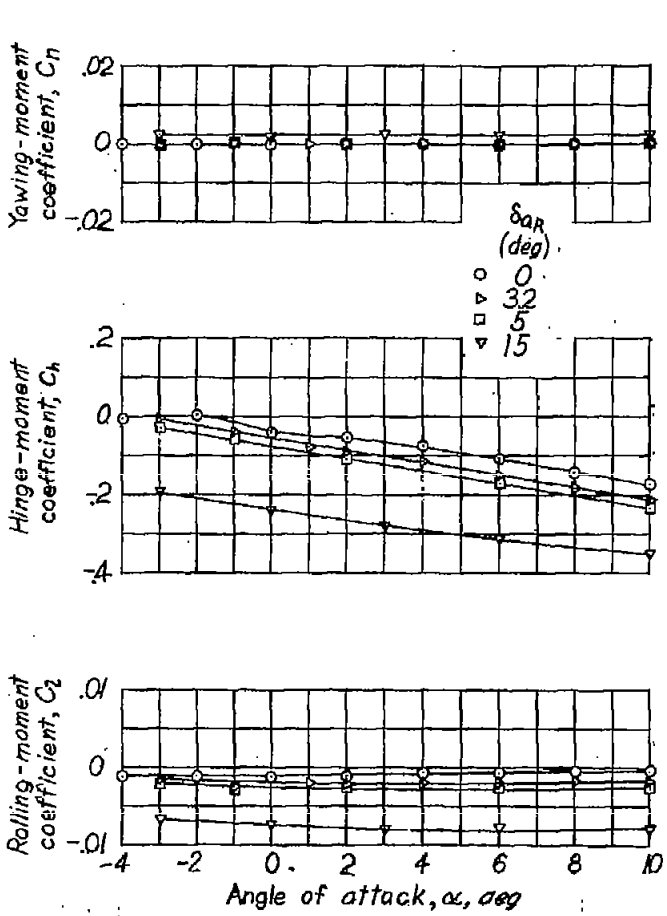

(a) Circular arc.

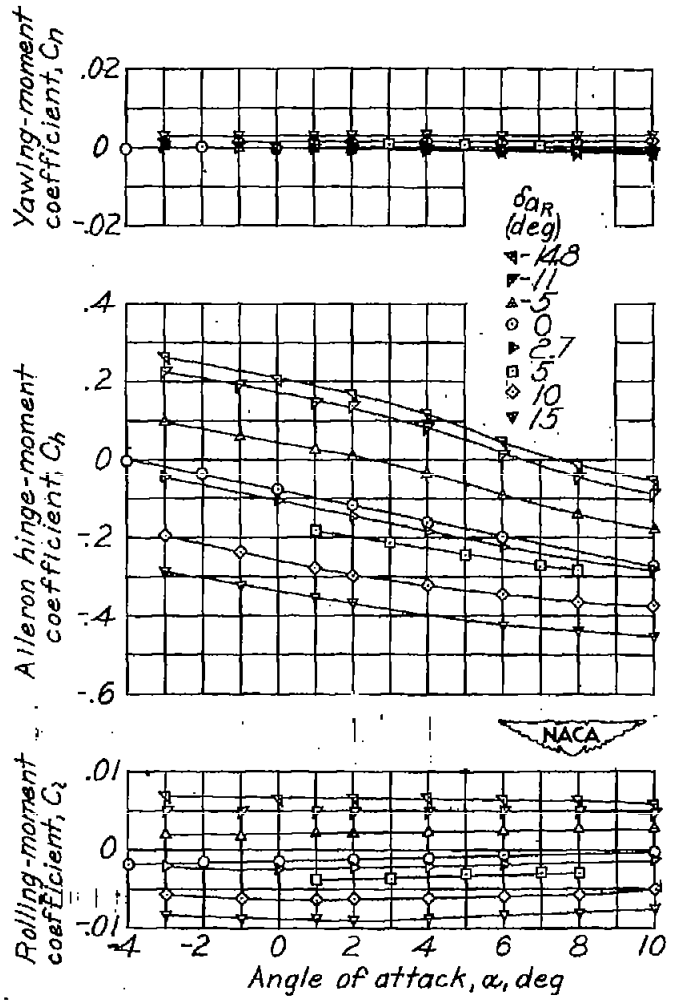

(b) t = 0.5.

Figure 10.- Effect of aileron deflection on the characteristics of a complete model equipped with various ailerons. M = 1.40.

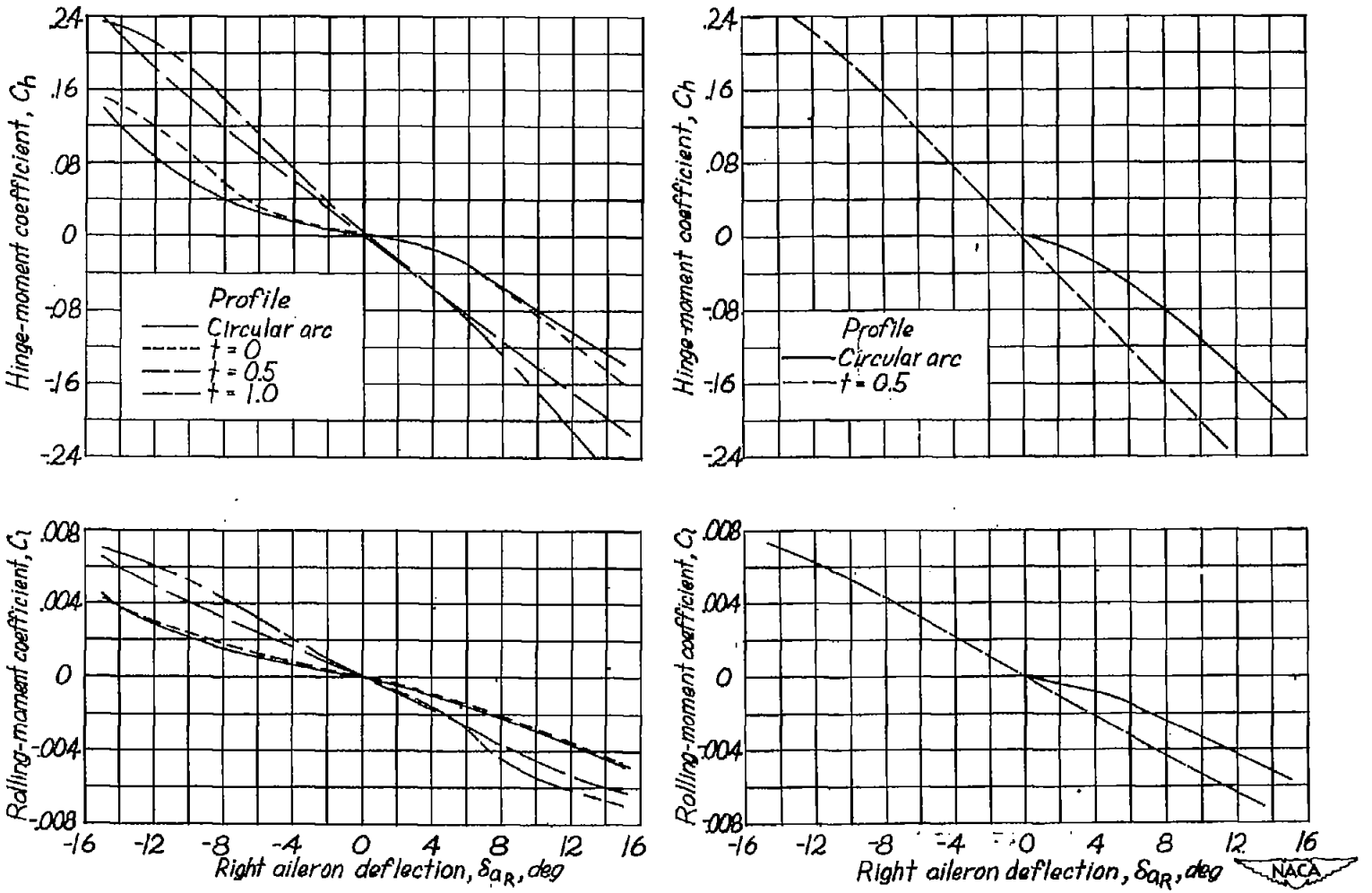

(a) M = 1.59. (b) M = 1.40.

Figure 11.- Effect of aileron profile on the rolling-moment and hinge-moment characteristics. $\alpha \approx -2.4^\circ$.

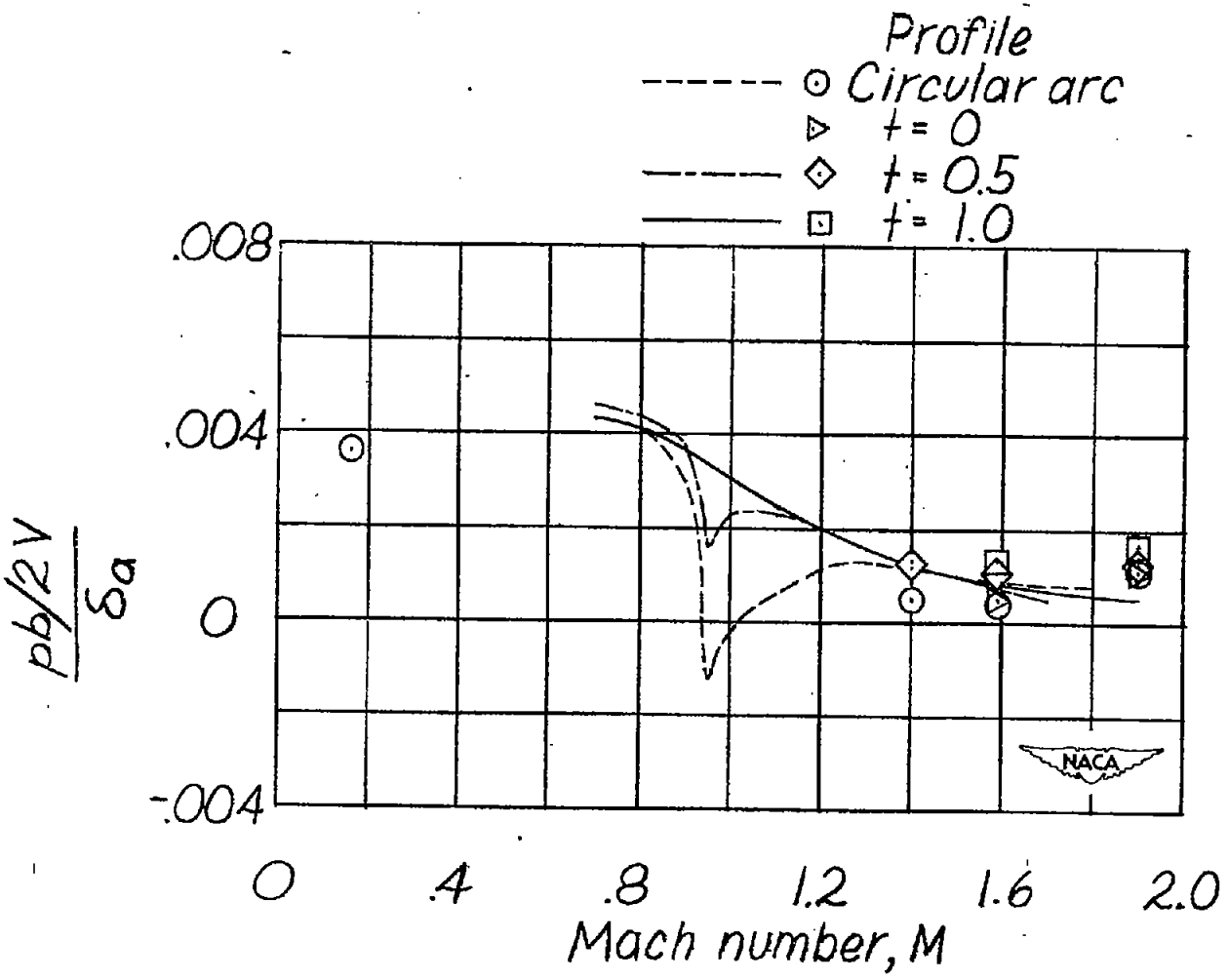

Figure 12.- Variation of $\frac{pb/2V}{\delta_a}$ with Mach number. Faired lines from rocket-model tests, symbols from wind-tunnel tests.

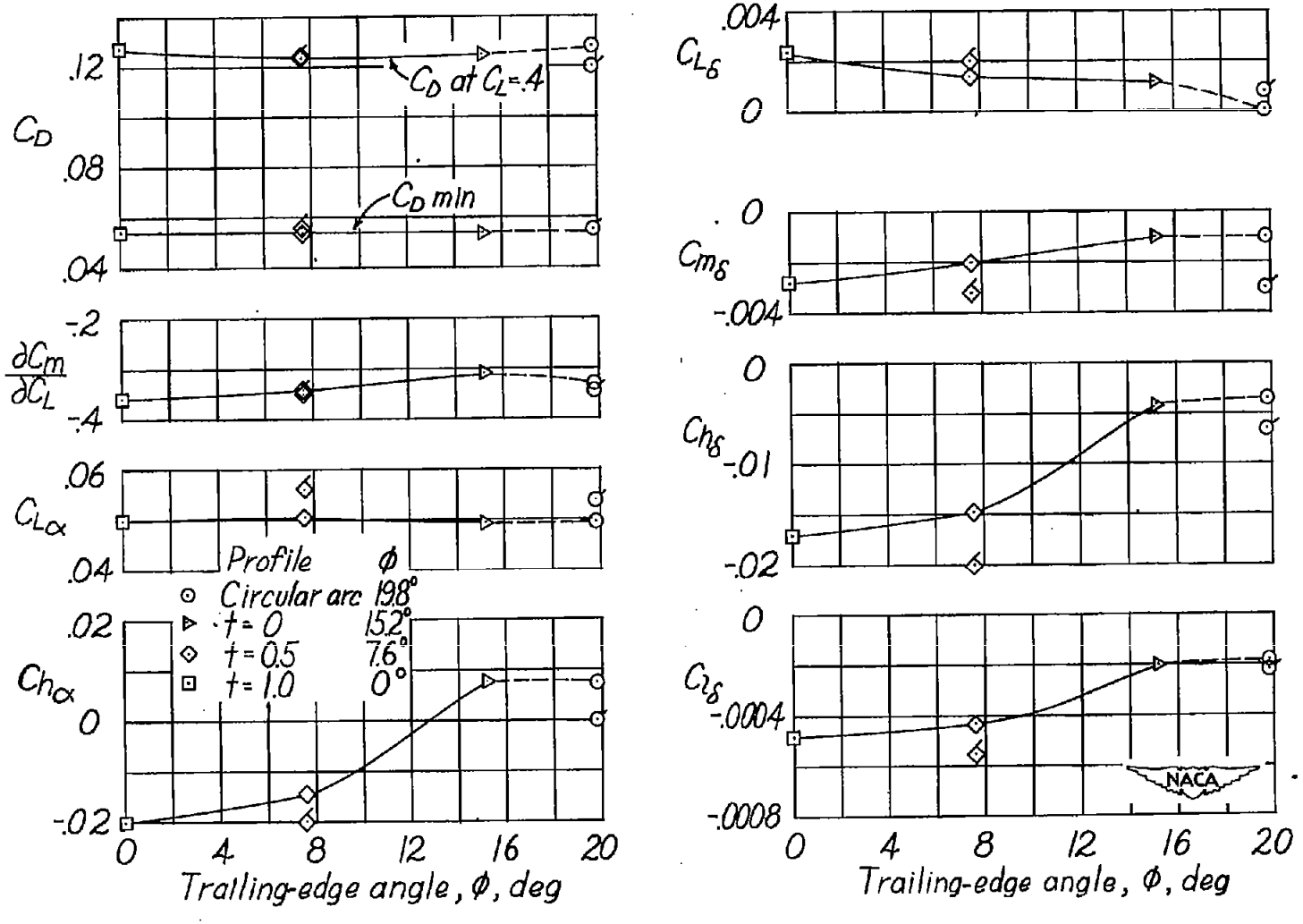

Figure 13.- Effect of trailing-edge angle on various aerodynamic characteristics. Faired line for M = 1.59; flagged symbols for M = 1.40.

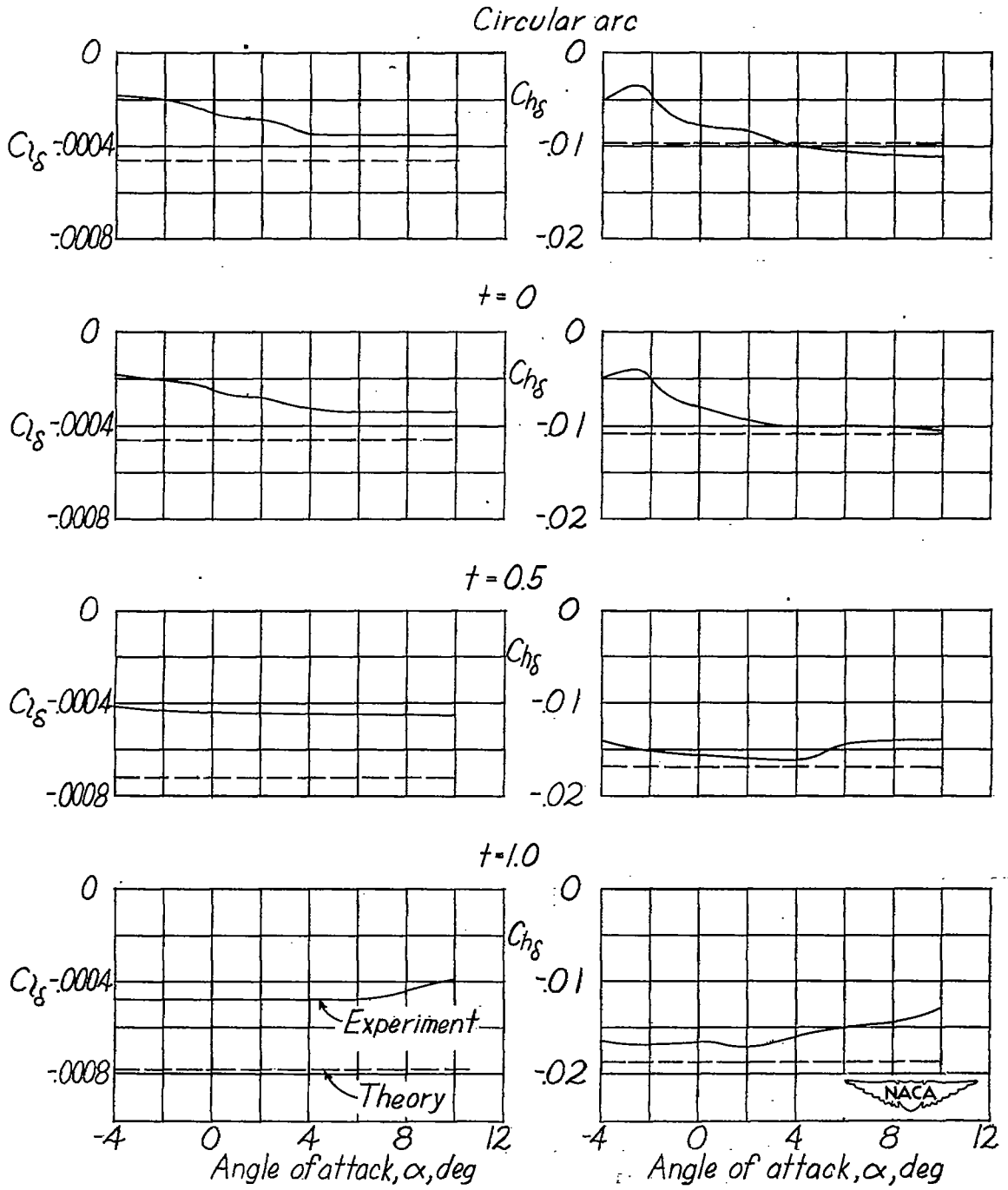

(a) M = 1.59.

Figure 14.- Variation of the experimental and theoretical values of C_{l_δ} and C_{h_δ} with angle of attack for various aileron profiles.

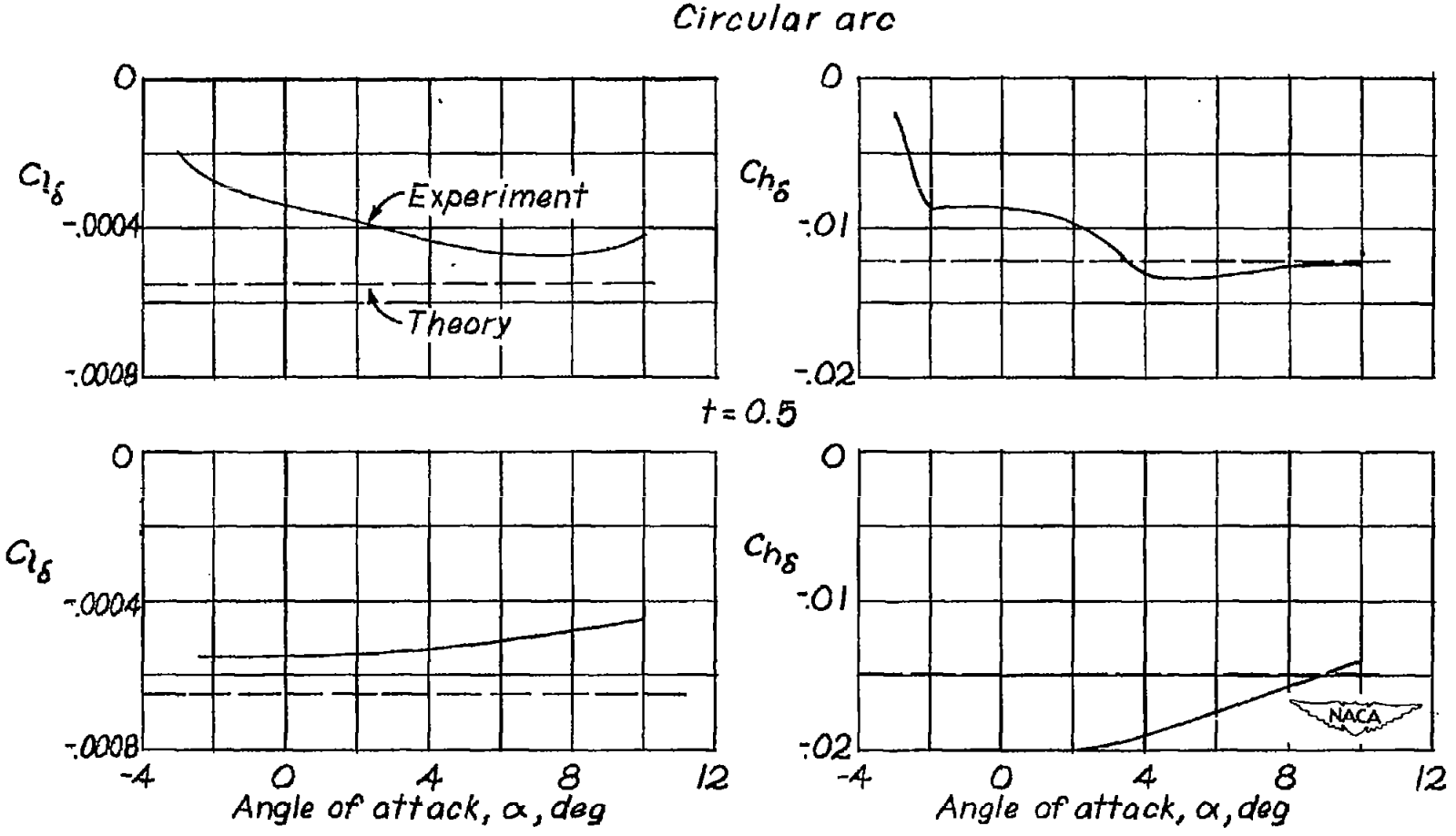

(b) M = 1.40.

Figure 14.- Concluded.

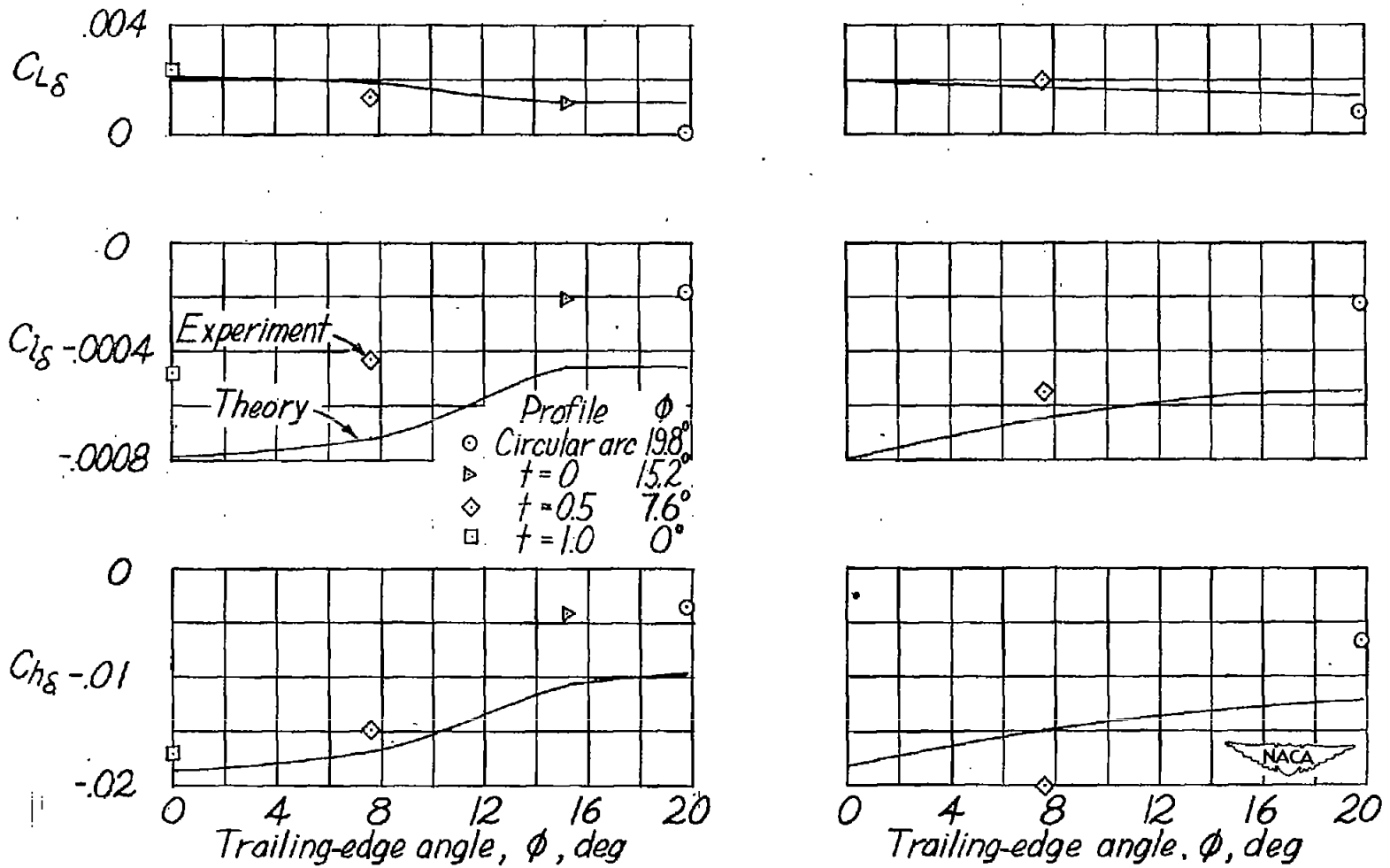

(a) M = 1.59. (b) M = 1.40.

Figure 15.- Comparison of theoretical and experimental aileron characteristics for various aileron profiles. $\alpha \approx -2.4°$.